AIAA JOURNAL
Vol. 46, No. 3, March 2008

# Truss Beam with Tendon Diagonals: Mechanics and Designs

Gyula Greschik*
*University of Colorado, Boulder, Colorado 80309*

DOI: 10.2514/1.25249

**A straightforward means to reduce the mass of a truss beam is to replace some of its rigid members with prestressed tendons. Such a solution, however, involves unique design considerations, most of which have been previously unaddressed in the literature. The present paper seeks to fill this gap by reviewing the general mechanics of and some specific design considerations for a basic class of such structures: regular triangular truss beams with tendon diagonals. The issues considered and illustrated in the context of three architectural options are the pretension necessary for tautness, member vibration, parasitic force effects, truss face accuracy, longeron compression eccentricities, and stiffness. This review offers not only design formulas for one redundant and two determinate variants of the considered class of trusses, but also a blueprint for the systematic analysis and design of other trusses with prestressed members. Two specific details of the involved derivations bear further significance: 1) some shear compliance formulas regularly used for truss beam Timoshenko continuum modeling are shown to be flawed and are corrected and 2) it is illustrated that structural asymmetry may be beneficial: the stiffness of an asymmetrically laced beam is shown to exceed that of its symmetric alternative.**

## Nomenclature

| | | |
|---|---|---|
| $A$, $I$ | = | cross-sectional area, moment of inertia |
| $C_e$ | = | local stability effective strength reduction coefficient due to the eccentricity of compression |
| $C_k$ | = | stiffness coefficient (auxiliary to the solution of the redundant design) |
| $d$, $r$, $t$ | = | tube diagonal, radius, and wall thickness |
| $E$, $\nu$ | = | Young's modulus, Poisson's ratio |
| $e$ | = | displacement |
| $e_P$ | = | eccentricity of longeron compression |
| $e_{\text{tip}}$ | = | half-truss-beam cantilever tip deflection |
| $F$, $P$ | = | truss member load (axial force) and compression $P = -F$ |
| $F_{\max,-p}$ | = | maximum member load without pretension effects |
| $F_{+\min}$ | = | minimum permissible tendon force |
| $f$ | = | vibration frequency |
| $J_1, \ldots, J_4$ | = | auxiliary constants in member load calculations |
| $\hat{K}$ | = | equivalent beam cross-sectional stiffness |
| $K_x$ | = | direct cross-sectional stiffness $EA$ in member $x$ |
| $L$ | = | truss beam length |
| $l$ | = | member length |
| $M$, $S$ | = | moment (bending moment), shear |
| $n$ | = | number of bays in truss beam |
| $P_{\text{eu}}$ | = | Euler load, $\pi^2 EI/l^2$ |
| $x$, $y$, $z$ | = | coordinate system aligned with the truss axis, lateral on the truss base, and up, respectively |
| $\mathbf{A}$, $\mathbf{B}$, ... | = | joints, truss edges, etc. |
| $\alpha_T$ | = | coefficient of thermal expansion |
| $\beta$ | = | rotational acceleration |
| $\gamma$, $\tau$ | = | shear deformation and stress |
| $\Delta_T$ | = | temperature difference |
| $\varepsilon_{\text{rms}}$ | = | truss face rms error, calculated with phased-array antenna relations |
| $\varepsilon_\Delta$ | = | strain (kinematic load) in the tendon diagonals relative to the struts |
| $\lambda$ | = | strut (longeron or batten) to tendon (diagonal) length ratio, $\lambda_i = l_i/l_d$ |
| $\rho_l$, $\rho_L$ | = | member and truss beam linear densities, mass/length |
| $\sigma$ | = | stress; direct stress |

*Subscripts*

| | | |
|---|---|---|
| $e$, $T$ | = | imperfection effects and thermal loads |
| $F$, $S$ | = | beam cross-sectional axial force and shear |
| $l$, $b$, $d$ | = | longeron, batten, and diagonal |
| $M$, $Q$ | = | beam cross-sectional bending moment and torque |
| $s$, $p$ | = | primary structural loads and prestress |

## I. Introduction

TENSION cord and cable members are not uncommon in trusses and frames: designs featuring such elements range from innovative high-rise buildings through spacecraft. Examples of the latter include precision applications such as tension truss [1] antennas (the AstroMesh [2] and other designs [3]), lightweight coilable lattice booms (the Astromast [4], the CoilABLE boom [5], and others [6]), more robust columns (the ADAM mast [7], etc. [8]), and surface lattices [9–11].

It should not be surprising that tendon truss members are so widely used. They are not only light and naturally immune to structural stability problems, but their compliance when unstressed (in stowage) permits their easy integration with a variety of stowage and deployment schemes. In fact, there are uniquely elegant deployment mechanisms (such as that of the Astromast [4]) that could not be realized without tendon members. An additional advantage of cord members in case of composite materials is near-optimal material stiffness, achieved by almost purely unidirectional construction (there is no structural need for cross fibers in a cord).

Despite these advantages and rich heritage, however, little about tendon-laced truss engineering itself is available in the literature. Although there are publications that discuss a few critical aspects of specific designs [4], the writer is unaware of any systematic review of practical or theoretical considerations, or of methodology, for the design of such structures.

This void may be due, in part, to the transparent elegance of most laced lattices, the mechanics of which tend to be deterministic and well-defined. The approximate or detailed analysis of such structures is rarely a formidable task. Despite this simplicity, however, there are

Presented as Paper 1945 at the 47th AIAA/ASME/ASCE/AHS/ASC Structures, Structural Dynamics, and Materials Conference, Newport, RI, 1–4 May 2006; received 18 May 2006; revision received 17 September 2007; accepted for publication 18 September 2007. 

*Research Associate, Center for Aerospace Structures, Department of Aerospace Engineering Sciences, UCB 429. Member AIAA.

issues and challenges characteristic, some even unique, to laced architectures that a designer should be keenly aware of. A systematic and detailed review of these points, even if often not conceptually novel or theoretically complex in the wider context of structures, has long been overdue.

To further this goal, the present paper offers a review of a number of issues typically confronted in laced truss beam design. The specific context of this summary is a fundamental, perhaps even archetypical, laced architecture: a regular triangular truss beam (Fig. 1) with tendon diagonals. Three variants of this structure are considered. These are the redundant cross-laced pattern (Fig. 2a) and two statically determinate singly laced two-bay patterns (Figs. 2b and 2c).

Similar to the indeterminate design, the first determinate pattern (Fig. 2b) has a 120-deg repetitive rotational symmetry about the truss axis $x$. The last pattern (Fig. 2c) is subsequently obtained by reversing bracing on one side (side **CA** in the figure). This reversal destroys rotational symmetry and introduces mirror symmetries between the modified side and its neighbors. (One-bay repetitive single-diagonal patterns are not considered because of their low shear stiffness.)

Considered for these designs are the extent of necessary pretension, the optimization of dominant member (tendon and strut) natural frequencies, the interaction of mission loads with parasitic forces (forces due to pretension and/or imperfections), how truss face accuracy is affected by member imperfections, how imperfections contribute to the eccentricities of longeron compression, and the calculation of resultant beam stiffness. The sections of the paper address one issue at a time: first those unique to laced designs, then the more generic concerns. Each topic is linked with the rest by the common context and a design example. Because of the general simplicity of the involved mechanics, the points made are only briefly explained, regardless of their practical significance. An exception is the assessment of effective (global equivalent) truss shear stiffness, a detailed derivation of which is necessary to sufficiently illuminate and then support the correction of a mistake in a seminal paper nearly three decades ago [12], one that continues to erroneously influence work to this day [13]. This derivation pivots on a careful illumination of the traditional and the proper use of some fundamental notions of beam mechanics and is presented in Appendix A.

## II. Construction, Loads, and the Defining Aspects of Mechanics

The first of the three designs considered, cross-laced construction with prestressed cords (Fig. 2a), is self-contained: by its redundancy, it can be internally loaded for cord tension with self-equilibrating forces. This is illustrated in Fig. 3a for an isolated side bay. By equilibrium, the forces $F_d$ in the two diagonals remain equal even if geometric or thermal perturbations occur. The latter effects change the tendon forces, but do so equally in both tendons (cf. thermal observations for the ADAM mast [7]).

A statically determinate structure, however, can be prestressed only externally. In most laced beams this is achieved with compressive "springs" (spreader elements loaded to elastically buckle). For example, the Astromast [4] employs elastically buckled spreaders in lieu of the battens in Fig. 2a. The spreaders then prestress the diagonals that consequently form a determinate skeleton with the longerons. Another well-known variant [6] of this architecture can be subsequently obtained by arranging the spreaders not where the battens are in Fig. 2a, but radially from the cross-sectional centers out to the longeron joints. This architecture can be further transformed into one in which even the longerons are tendons [14], if the spreader joints at the cross-sectional centers are linked to one another along the truss with struts.

Unlike the examples just cited, the configurations in Figs. 2b and 2c derive from the redundant design (Fig. 2a) by diagonal, not batten, elimination. Unless elastic spreaders are inserted between the endpoints of each remaining diagonal, diagonal tension in such a structure calls for pulling the other pair of bay joints (from where diagonals were removed) toward one another (Fig. 3b). This can be achieved with a compliant tension element: for example, a prestressing cord with a constant-force (CF) spring (Fig. 3c). Thus prestress with tension, rather than compression, springs is realized.

Such tensioning with a compliant cross-diagonal line is implied in both determinate designs considered in this paper (Figs. 2b and 2c), even if the prestressing cords are not depicted in the figures. These beams thus ultimately differ from the cross-laced beam (Fig. 2a) only by the dramatically lower stiffness of some of their diagonal cords: stiffness so low that these cords can no longer be called members, but tension springs. These cords, nevertheless, are located in the hardware exactly where the extra tendon diagonals are in the cross-laced truss. In physical reality, therefore, the three designs all offer the view shown in Fig. 4; they may appear quite similar to a casual observer. The fundamental mechanical differences are "hidden," apparent only upon closer hardware inspection.

By their geometric similarity, the three designs develop the same member loads (Table 1) upon pretensioning. The loads due to other effects, however, are different: these include the primary operational (such as maneuvering) loads and, for the redundant truss, those due to imperfection and thermal effects.

Prestress also affects deployment: the means to deploy either considered structure must be more forceful than what the deployment technology would otherwise require. The loads to be ordinarily overcome during deployment stem from contact and hinge friction, elastic and inelastic deformation effects, and possibly from the need to prestress some components for space rigidization and to overcome thermal-imperfection effects. To deploy a prestressed truss, however, the deployment mechanism must overcome these technological loads with the pretension (Table 1) combined. The load overhead by pretension naturally and directly depends on the diagonal prestress, which in turn depends on other load effects, as seen below.

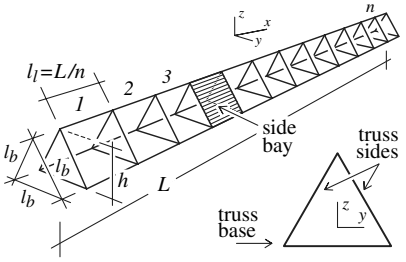


**Fig. 1 Truss beam skeleton.**

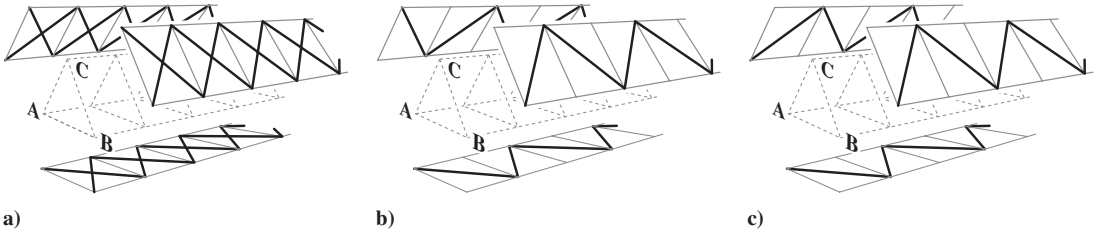


**a)** **b)** **c)**

**Fig. 2 Three bracing options.**

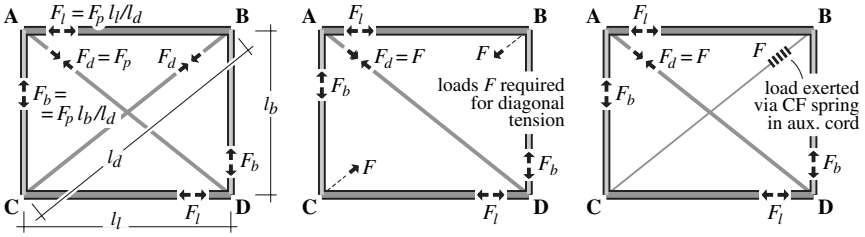


a) Cross diagonals b) Single diagonal c) Prestressing cord

**Fig. 3 Prestressing mechanics in isolated bay.**

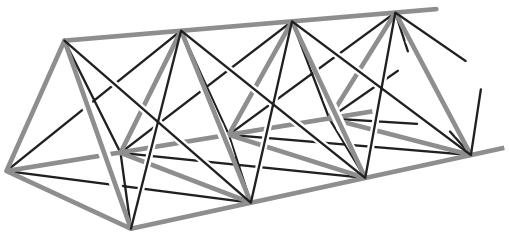

**Fig. 4 Truss view.**

## III. Considerations Unique to a Pretensioned Truss

The use of tendon members entails two special mechanical issues beyond the more generic strength, stiffness, and weight efficiency (performance) concerns. First, each cord must be prestressed enough to remain taut in all operating states. Obviously, if this condition is violated, the tendon slackens and fails to function as a member, jeopardizing truss integrity. However, there is another, more subtle, mechanical issue to also affect the design: a coupling between tendon and strut member vibration frequencies. Pretension concurrently raises cord and lowers strut vibration frequencies. There exists a level of prestress at which the dominant frequencies for tendons and struts coincide: an optimum that achieves the highest possible governing frequency for all members.

### A. Pretensioning for Tautness

Because of linear behavior typical in space applications, a member load $F$ is a simple sum of responses to prestress, primary structural loads (slewing, etc.), and thermal-imperfection effects $F_p$, $F_s$, and $F_{eT}$:

$$F = F_p + F_s + F_{eT} \tag{1}$$

The signs of the last two components ($F_s$ and $F_{eT}$) can vary: $F_i \epsilon [-F_{i,\max}, +F_{i,\max}]$. The first two components ($F_p$ and $F_s$) are usually deterministic, and the last ($F_{eT}$) is of a statistical nature.

For a tendon member (assumed in the following), the $F_p$ response component in Eq. (1) is the pretension itself ($F_d = F$ in Fig. 3). For tautness, the tendon force $F$ must be greater than a safe margin:

$$F > F_{+\min} > 0 \tag{2}$$

This condition guarantees structural integrity.

**Table 1 Loads due to diagonal pretension $F_p$ for both redundant and determinate designs.**

| Member | Member force In general | Member force If $l_b = l_l$ |
|---|---|---|
| All diagonals | $F_p$ | $F_p$ |
| All longerons | $-F_p 2\lambda_l$ | $-F_p\sqrt{2}$ |
| Battens at truss end | $-F_p\lambda_b$ | $-F_p/\sqrt{2}$ |
| Intermediate battens | $-F_p 2\lambda_b$ | $-F_p\sqrt{2}$ |

Considering Eq. (1) and the variability of the signs of $F_s$ and $F_{eT}$, Eq. (2) can be rewritten to express tendon pretension $F_p$ as

$$F_p > F_{+\min} + F_{s,\max} + F_{eT,\max} \tag{3}$$

Components $F_{i,\max}$ in this criterion depend on the design, hardware construction, primary structural loads, and environmental conditions. For a statically determinate structure in which thermal and imperfection effects do not load the members ($F_{eT,\max}$ disappears), this integrity condition reduces to

$$F_p > F_{+\min} + F_{s,\max} \tag{4}$$

Substituting $F_p$ of Eq. (3) [alternatively, Eq. (4)] into Eq. (1), one obtains

$$F_p = F_{+\min} + \sum_{i=s,eT} (F_{i,\max} + F_i) \tag{5}$$

Then, noting that $F_{i,\max}$ are the extrema of $F_i$, the maximum tendon force $F_{\max}$ can be expressed as

$$F_{\max} = F_{+\min} + 2\sum_{i=s,eT} F_{i,\max} = F_{+\min} + 2F_{\max,-p} > 2F_{\max,-p} \tag{6}$$

where $F_{\max,-p}$ is the maximum possible cord response to all effects except prestress. Apparently, for a tendon to be used in lieu of a strut, its extreme load after sufficient pretensioning will be at least twice that associated with an equivalent strut with no prestress applied.

Because imperfection and thermal effects can significantly contribute to compression in the battens in the redundant design (Fig. 2a), the observation just made also implies that diagonal pretensioning will roughly double the extreme compression in these struts.

### B. Pretension to Synchronize Governing Cord and Strut Frequencies

To consider how tendon and strut vibration frequencies depend on prestress, begin with the expression [15,16] for the $i$th natural frequency $f_i$ of a strut (beam column) of linear density $\rho_l$ under tension $F$ with pin-supported ends:

$$f_i = \sqrt{1 + Fl^2/(EI(i\pi)^2)}\,\sqrt{EI/\rho_l}(i\pi)^2/(2\pi l^2) \tag{7}$$

Consequently, the natural frequencies of a tendon (no flexural stiffness) are

$$f_i = \sqrt{F/\rho_l}\, i/(2l) \tag{8}$$

The general expression (7) can also be written as

$$f_i = \sqrt{i^2 + F/P_{\text{eu}}}\,\sqrt{EI/\rho_l}(i\pi)/(2l^2) \tag{9}$$

to reveal that the dominant strut natural frequency is proportional to $\sqrt{1 + F/P_{\text{eu}}}$ (with $F < 0$ for compression).

The vibration frequency of any member can be calculated by placing these equations in the context of the considered architectures. Because the level of prestress affects tendon and strut frequencies in opposite ways, the dominant (lowest) vibration frequency of the combined set of struts and tendons is maximized when tendon and

strut frequencies are equal. To calculate the prestress $F_{p,f}$ to achieve this optimum, first substitute the cord length $l_d$, tendon linear density $\rho_{l,d}$, and $P_{p,f}$ for $l$, $\rho_l$, and $F$ in Eq. (8). Then, considering Table 1, replace $F$ in Eq. (9) with $-2P_{p,f}l/l_d$. (For now, let the member length $l$ and linear density $\rho_l$ in the latter relation remain generic.) Subsequently equating the frequencies by the two equations and rearranging yields

$$F_{p,f} = P_{\text{eu}}/[2\lambda + (\rho_l/\rho_{l,d})\lambda^2] \tag{10}$$

in which $\lambda$ is the strut-to-tendon-length ratio. For similar tendon and strut material densities and negligible nonstructural masses, then

$$F_{p,f} \approx P_{\text{eu}}/[2\lambda + (A/A_d)\lambda^2] \tag{11}$$

where $A$ denotes the cross-sectional area. For $\lambda = 1/\sqrt{2}$ (square side bays), Eq. (11) further simplifies to

$$F_{p,f} \approx P_{\text{eu}}/[\sqrt{2} + A/(2A_d)] \tag{12}$$

If diagonal prestress in any considered design (Fig. 2) is $F = F_{p,f}$, then the dominant tendon frequency will match that of the strut, the parameters of which ($\lambda$, $\rho_l$ or $A$, and $P_{\text{eu}}$) are used in Eqs. (10–12). Because, via their typically lower stiffness, the battens will likely dominate strut vibration effects, one may want to use $\lambda = \lambda_b$, $\rho_l = \rho_{L,b}$, $A = A_b$, and $P_{\text{eu}} = P_{\text{eu},b}$.

Pretension according to Eqs. (10–12) maximizes the governing dominant truss member (tendon or strut) vibration frequency. For other values, either a tendon or a strut dominant frequency will drop below the optimum (higher pretension reduces strut, lower pretension reduces cord, frequencies).

## IV. Further Design Considerations

Of the more generic issues that are not unique to laced structures, kinematics and member loads due to thermal and imperfection effects and loads due to slewing are here reviewed. These details influence the necessary level of prestress [Eq. (3)] and also offer insight for a comparative analysis of the design alternatives considered.

Imperfections and thermal loads are modeled as uniform tendon strains with respect to the rest of the structure. It is thus assumed that all members respond to thermal loads and are subject to dimensional errors uniformly within their own respective classes: all tendons undergo the same strain and so do all struts (the kinematic responses of the two sets may differ). This approach is fit either for a simple approximate analysis or for the assessment of a worst-case scenario. In the design example subsequently discussed, a study of the latter, worst-case scenario, will be implied.

### A. Parasitic Internal Loads

A redundant structure (Fig. 2a) responds to kinematic loads (geometric errors or thermal effects) with deformations constrained by internal loads. If the kinematic effect is a uniform tendon strain $\varepsilon_\Delta$, then the diagonals, battens, and longerons will develop the following self-equilibrating set of loads:

$$F_{d,eT} = -\varepsilon_\Delta/C_k \tag{13}$$

$$F_{b,eT} = 2\varepsilon_\Delta\lambda_b/C_k \tag{14}$$

$$F_{l,eT} = 2\varepsilon_\Delta\lambda_l/C_k \tag{15}$$

$$C_k = 1/K_d + 2\lambda_b^3/K_b + 2\lambda_l^3/K_l \tag{16}$$

in which $K_i$ denotes the direct cross-sectional stiffness $EA_i$ of member $i$, and the subscripts $T$ and $e$ indicate combined thermal and imperfection effects. These loads, with their signs variable according to that of $\varepsilon_\Delta$, parasitically add to the other (prestressing and slewing) member loads. The truss beam does not deform laterally.

If in a redundant design the kinematic effects contribute to the necessary pretension more than other structural loads, then the thermal-imperfection term $F_{eT,\max}$ dominates Eq. (3). In this case, the level of pretension needed is much higher than for a determinate design; high strut loads also result. Pretensioning effectively magnifies the parasitic load effects associated with redundancy.

### B. Deformations from Thermal-Imperfection Effects

Contrary to the redundant case, the response of a determinate design to kinematic loads involves only deformations and no internal loads. These deformations are herein considered in terms of the truss base (lower face) kinematics, in the context of a repetitively identical two-bay truss unit. In particular, the displacements of the truss face joints between the two bays are assessed with respect to the unit ends. This kinematic response is shown in Figs. 5a and 5b for the architectures of Figs. 2b and 2c, respectively. Additionally, Fig. 5c depicts the latter architecture turned to its side: the base here is side **CA**, for which the diagonal pattern is reversed. (Here, the pattern of diagonals on the two sides of a longeron is mirror-symmetric along truss edges **A** and **C** on the base, but it is asymmetric on the "rooftop" edge **B**.) For these configurations, the displacement expressions applicable to trusses with square bays are listed in Table 2.

The results reveal that the truss base out-of-plane deformations are most benign for the design with disturbed symmetry if the diagonal pattern is reversed on the base (Fig. 5c). Somewhat more severe are the deformations for the same design oriented as in Figs. 2c and 5b and most severe are the deformations for the rotationally symmetric case in Figs. 2b and 5a.

To highlight this relative order in surface accuracy in terms of the geometric performance metrics of a presumed phase-array antenna surface on the truss base, the rms surface errors can be calculated [17] via

$$\varepsilon_{\text{rms}} = \left[\int (z_{\text{srf}} - z_0)^2 \, \mathrm{d}A/A\right]^{1/2} \Big/ 2 \tag{17}$$

where $z_{\text{srf}} = z_{\text{srf}}(x, y)$ is the actual truss face and $z_0 = z_0(x, y)$ is the ideal truss face: the plane that minimizes $\varepsilon_{\text{rms}}$. For the deformation patterns shown in Fig. 5, respectively, Eq. (17) reduces to the expressions

$$\varepsilon_{\text{rms},a} = \varepsilon_\Delta l_d\sqrt{27}/(36\lambda_b) \tag{18}$$

$$\varepsilon_{\text{rms},b} = \varepsilon_\Delta l_d\sqrt{39}/(36\lambda_b) \tag{19}$$

$$\varepsilon_{\text{rms},c} = \varepsilon_\Delta l_d\sqrt{3}/(36\lambda_b) \tag{20}$$

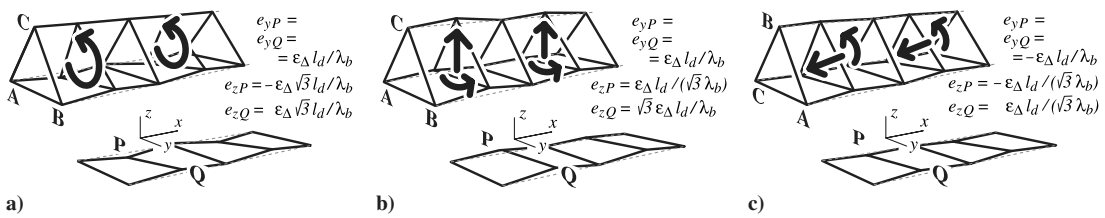


a) b) c)

**Fig. 5 Deformations from uniform strain $\varepsilon_\Delta$ in all diagonals; architecture of a) Fig. 2b, b) Fig. 2c, and c) Fig. 2c, sideways.**

**Table 2 Base node displacements for truss with square bays ($l_b = l_l$ and $\lambda_b = \lambda_l = 1/\sqrt{2}$; Fig. 5)**

| Design | Figure 2b | Figure 2c | |
|---|---|---|---|
| | | As shown | Base is **AC** |
| $e_{yP} = e_{yQ}$ | $1.414\varepsilon_\Delta l_d$ | $1.414\varepsilon_\Delta l_d$ | $-1.414\varepsilon_\Delta l_d$ |
| $e_{zP}$ | $-2.449\varepsilon_\Delta l_d$ | $.8165\varepsilon_\Delta l_d$ | $-.8165\varepsilon_\Delta l_d$ |
| $e_{zQ}$ | $2.449\varepsilon_\Delta l_d$ | $2.449\varepsilon_\Delta l_d$ | $.8165\varepsilon_\Delta l_d$ |

As previously seen in terms of the joint displacements, geometric performance for Figs. 2b and 2c is, respectively, the least and most sensitive to the kinematic loads considered.

*1. Eccentricity*

In some situations, the kinematics discussed previously may not only contribute to truss inaccuracy, but can also influence member strength. This happens if the longerons are clamped to the truss joints: a construction that renders them structurally continuous, making them work as long, multiply supported, beam columns. Lateral joint displacements $e_P$, consequently, become longeron compression eccentricities, which add flexure to member compression. The maximum value of this eccentricity (the worst combination of the $x$ and $y$ displacements shown in Fig. 5) turns out to be

$$e_P = 2\varepsilon_\Delta l_d/\lambda_b = 2\varepsilon_\Delta L/(n\lambda_l\lambda_b) \tag{21}$$

for both determinate architectures. [For the rotationally symmetric option (Fig. 2b) all midunit joints (Fig. 5a) move with $e_P$. In the case with mirror symmetries (Fig. 2c), the joint across the side with the diagonals reversed (joint **Q** in Fig. 5b) is displaced with $e_P$.]

Because both global and local [18] stability limits for thin-walled tubes can be defined in terms of the maximum axial stress, the coefficient of *reciprocal stress increase* due to eccentricity $e_P$ can be used to quantify effective member strength reduction. This coefficient, herein denoted as $C_e$, can be derived by combining compression and eccentricity-induced flexure in the context of a circular cross section to yield

$$-\sigma_{\max} = (P/A)/C_e \tag{22}$$

$$C_e = 1/(1 + e_P/r) \tag{23}$$

where $r$ is the tube radius. Further combining this result with Eq. (21), one obtains

$$C_e = 1/[1 + (2\varepsilon_\Delta L)/(nr\lambda_l\lambda_b)] \tag{24}$$

In terms of the bay shapes, the extrema of this coefficient coincide with those of the product $\lambda_l\lambda_b$. Longeron strength reduction, therefore, is the most benign ($C_e \to \max$) for square side bays ($\lambda_l\lambda_b \to \max$, when $\lambda_l = \lambda_b = 1/\sqrt{2}$).

Note that the longeron flexure associated with joint displacements somewhat constrains the ideal kinematics just assumed. Although not likely to *significantly* affect the eccentricities, this constraint makes Eq. (21) predict the eccentricity as an upper bound, $e_{P,\max}$, rather than the precise value. The $C_e$ coefficient according to Eq. (24) is, therefore, a conservative approximation.

### C. Primary Structural Loads

To assess member loads due to slewing, consider steady-state rotational acceleration $\beta$ about the truss beam midspan and denote truss beam linear mass with $\rho_L$. (To account for transient effects, $\beta$ can be increased above that value associated with the nominal maneuvering kinematics.) The extreme truss beam cross-sectional moment $M$ and shear $S$, at midspan, thus become

$$M = \beta\rho_L L^3/24 \tag{25}$$

$$S = \beta\rho_L L^2/8 \tag{26}$$

Member responses to these loads for two perpendicular slewing orientations are listed in Table 3, according to the truss and cross-sectional orientations shown in Figs. 1 and 2. The $\pm$ and $\mp$ symbols reflect alternative diagonal orientations.

## V. Design Example

To illustrate the relations derived previously, consider a truss beam of length $L = 100$ m with $n$ square side bays: $l_l = L/n$ and $l_l/l_b = 1$, with $\lambda_l = \lambda_b = 1/\sqrt{2}$. Further, let all structural materials have Young's modulus, Poisson's ratio, and density of $E = 68.948$ GPa, $\nu = 0.3$, and $\rho = 1660$ kg/m$^3$, respectively, with coefficients of thermal expansion of $\alpha_T = 1$ ppm/°C. Use tubular longerons and battens with $t_l = .2134$ mm and $t_b = .5334$ mm wall thicknesses, and $d_l = 12.7$ cm and $d_b = 3.81$ cm diameters, respectively. The longeron and batten member properties are as shown in Table 4, and the coefficient $C_k$ [Eq. (16)] becomes

$$C_k = 2.529 \times 10^{-6}\,1/\mathrm{N} \tag{27}$$

Next, let the tendons (of a material similar to the struts) have $12.7 \times 0.508$ mm cross sections of $A_d = 6.452$ mm$^2$ area and $K_d = (EA)_d = 444.8$ kN stiffness. For a safe margin over slackness, require the tension in the tendon to be at least $F_{+\min} = 0.5$ N. The batten Euler load $P_{\mathrm{eu},b}$ and, consequently, the dynamically optimal pretension $F_{p,f}$ (to synchronize tendon and batten frequencies [Eq. (12)]) are then both proportional to the square of the bay number $n$:

**Table 3 Member loads at midspan (truss beam length $L$ and linear density $\rho_L$) from slewing with rotational acceleration $\beta$ [compare with Eqs. (25) and (26) and Fig. 2]**

| Design | Redundant (Fig. 2a)[b,c,d,e] | | Determinate 120-deg rotational symmetry (Fig. 2b)[b,c] | | Determinate limited mirror symmetry (Fig. 2c)[b,c] | |
|---|---|---|---|---|---|---|
| Slew plane | $x-z$ | $x-y$ | $x-z$ | $x-y$ | $x-z$ | $x-y$ |
| Longeron **A**[a] | $+J_1' Dn$ | $-J_1 n\lambda_l/6$ | $+2J_1' n\lambda_l$ | $-J_1 n\lambda_l/6$ | $+2J_1' n\lambda_l$ | $-J_1 n\lambda_l/6$ |
| Longeron **B**[a] | $+J_1' J_3 n$ | $+J_1 n\lambda_l/6$ | $+2J_1' n\lambda_l$ | $+J_1 n\lambda_l/6$ | $+2J_1' n\lambda_l$ | $+J_1 n\lambda_l/6$ |
| Longeron **C**[a] | $-2J_1' J_3 n$ | 0 | $-4J_1' n\lambda_l$ | 0 | $-4J_1' n\lambda_l$ | 0 |
| Diagonal **AB** | $\pm 2J_1' J_4 n$ | $\pm J_1/6$ | 0 | $\pm J_1/3$ | 0 | $\pm J_1/3$ |
| Diagonal **BC** | $\mp J_1'(J_4 n \pm 3)$ | $\pm J_1/12$ | $\pm 6J_1'$ | $\pm J_1/6$ | $\pm 6J_1'$ | $\pm J_1/6$ |
| Diagonal **CA** | $\mp J_1'(J_4 n \pm 3)$ | $\pm J_1/12$ | $\mp 6J_1'$ | $\pm J_1/6$ | $\pm 6J_1'$ | $\mp J_1/6$ |
| Batten **AB** | $\mp 4J_1' J_4 n\lambda_b$ | 0 | 0 | 0 | 0 | 0 |
| Batten **BC** | $\pm 2J_1' J_4 n\lambda_b$ | 0 | 0 | 0 | 0 | 0 |
| Batten **CA** | $\pm 2J_1' J_4 n\lambda_b$ | 0 | 0 | 0 | 0 | 0 |

[a]Some of the longeron loads listed overestimate the precise value with a factor of up to $1 + 2/n$. The longerons with these errors depend on the slewing direction and the diagonal orientation at midspan.
[b]$J_1' = J_1/(12\sqrt{3})$.
[c]$J_1 = \beta\rho_L L^2/(4\lambda_b)$.
[d]$J_3 = 2\lambda_l/(J_2 + 3)$, where $J_2 = 1/[1 - 2\lambda_l^3/(K_l C_k)]$.
[e]$J_4 = J_2\lambda_l^3/[K_l C_k(J_2 + 3)]$, where $J_2 = 1/[1 - 2\lambda_l^3/(K_l C_k)]$.

$$P_{\mathrm{eu},b} = \pi^2 n^2 EI_b/L^2 \approx 0.7883n^2 \text{ N} \tag{28}$$

$$F_{p,f} = P_{\mathrm{eu},b}/[\sqrt{2} + A_b/(2A_d)] \approx 0.1239n^2 \text{ N} \tag{29}$$

### A. Environmental Loads, Imperfections, and Slewing

Assuming different environmental conditions (levels of thermal protection) and different thermal structures for tendons and struts, take a $\Delta_T = 100°\text{C}$ maximum temperature difference between the two; this entails $\varepsilon_{\Delta T} = \pm.0001$ relative strain. Further assume fabrication errors half this magnitude, $\varepsilon_{\Delta e} = \pm.00005$; this corresponds to 2-mil errors over each 1-m member length as the worst combination of cord- and strut-length errors, as well as joint imperfections. Thus, the worst-case kinematic load is an

$$\varepsilon_\Delta = \varepsilon_{\Delta T} + \varepsilon_{\Delta e} = \pm.00015 \tag{30}$$

relative tendon strain. And the parasitic diagonal, batten, and longeron loads for the redundant design, via Eqs. (13–15), are

$$F_{d,eT} = \mp 59.31 \text{ N} \tag{31}$$

$$F_{b,eT} = \pm 83.87 \text{ N} \tag{32}$$

$$F_{l,eT} = \pm 83.87 \text{ N} \tag{33}$$

The maximum eccentricity of longeron compression in units of meter, via Eq. (21), and the resulting member strength reduction coefficient are then

$$e_{P,\max} = .060/n \tag{34}$$

$$C_e = 1/(1 + .945/n) \tag{35}$$

For a quantitative assessment of maneuvering loads, assume truss beam linear mass $\rho_L = 15$ kg/m (total system mass: 1500 kg) and rotational acceleration $\beta = 10^{-3}$ rad/s$^2$ (acceleration, then deceleration, with this value turns the system with 90 deg in about 79 s). The auxiliary constants used in Table 3 thus become $J_1 = 53.03$ N, $J_1' = 2.552$ N, $J_2 = 1.050$, $J_3 = .3492$, and $J_4 = .006175$. (The truss beam linear mass should, as assumed, be independent of the number of bays and of the truss cross-sectional dimensions, because the member cross sections do not depend on the member lengths.) According to Table 3 and these parameters, the maximum member force magnitudes consequently become as listed in Table 5.

### B. Comparison of Design Alternatives

For a general review and comparison of the considered architectures, the equations derived previously are herein placed in the contexts of bay numbers $n = 30$, 60, and 90. These values correspond to $l_l = l_b =$ 3.333-, 1.667-, and 1.111-m bay and strut lengths.

Begin with calculating from Table 5 the maximum tendon load magnitudes from slewing and, from Eq. (31), the parasitic tendon loads: the first two lines in Table 6. Adding these to the minimum tendon tension $F_{+\min} = 0.5$ N according to Eq. (3), one obtains the required diagonal pretension $F_p$ (row 3). Apparently, the parasitic loads in the redundant design due to thermal and imperfection effects call for a prestress more than three times that needed in either determinate alternative. Redundancy is penalized to an even more severe extent in terms of the consequent total extreme member loads, shown in row 4 for the tendons, $F_{\max,d}$, according to Eq. (6).

Listed in the next row is the dynamically optimal pretension $F_{p,f}$ according to Eqs. (10) and (29). (This prestress equates tendon and batten dominant frequencies.) The required minimum prestresses for the 30-bay redundant designs, 136.8,. . .,137.3 N, are well over this threshold $F_{p,f} = 111.5$ N. For these designs, batten, rather than tendon, vibration governs member dynamics. Such a situation could occur for bay numbers 60 and 90 as well, if the member cross sections were not held constant for all truss geometries but would scale with the bay dimensions.

The batten Euler loads, in the next line, are listed for reference only. Their values are all safely above the actual extreme member compressions.

However, the extent of longeron strength reduction due to thermal-imperfection-induced eccentricities in the determinate designs, listed next according to Eq. (24), is noteworthy. Although one might generally presume that this effect is insignificant, the present results indicate that this may not always be so. Despite the large longeron diameters (here, longeron $L/D \approx 26$, even for $n = 30$), the strength degradation can exceed 3%. Reducing longeron diameters to $d_l = 64.5$ mm, half the current values (which results in still a rather stout member, $L/D \approx 52$), the strength reduction coefficient would further drop to $C_e = 0.94$, a 6% strength degradation. This effect should not be overlooked.

The imperfection- and thermal-effected parasitic longeron loads $F_{d,eT}$, again apply only to the redundant design [Eq. (15)]. These loads combine with the longeron prestress $F_{l,p} = 2F_p\lambda_l$ to constitute the maximum longeron load during deployment, $F_{l,\mathrm{depl}}$. (It is assumed that the structure is not maneuvered during deployment.) These loads directly penalize deployment: they need to be overcome by the deployment mechanism in addition to the regular loads associated with the deployment method used. (The latter include tribological effects and the possible need for member-level prestress such as pressurization if space rigidization is used.) This penalty is nearly an order of magnitude greater for the redundant designs.

Listed last are the antenna base surface rms errors from thermal-imperfection effects alone, according to Eqs. (18–20). The configuration with mirror-symmetric sides is clearly the least favorable option as far as antenna face precision is considered. Not included in the table is the design with perturbed symmetry on its side (Fig. 5c), the surface accuracy of which is by far the least affected by the kinematic loads.

**Table 4 Strut cross-sectional properties**

| Member | Longerons | Battens | |
|---|---|---|---|
| Cross section | | | |
| Area $A$ | 85.126 | 63.844 | mm$^2$ |
| Moments of inertia $I$ | 171,620 | 11,585 | mm$^4$ |
| Direct stiffness $EA$ | 5869 | 4402 | kN |
| Flexural stiffness $EI$ | 11.833 | 0.7987 | kN · m |
| Member lin. density $\rho_l$ | 0.1413 | 0.1060 | kg/m |

**Table 5 Maximum member load magnitudes (N) from slewing for the example problem (cf. Table 3)**

| Design | Redundant (Fig. 2a) | | Determinate 120-deg rotational symmetry (Fig. 2b) | | Determinate limited mirror symmetry (Fig. 2c) | |
|---|---|---|---|---|---|---|
| Slew plane | $x$–$z$ | $x$–$y$ | $x$–$z$ | $x$–$y$ | $x$–$z$ | $x$–$y$ |
| Longerons **A** and **B** | $0.8910n$ | $6.250n$ | $3.608n$ | $6.250n$ | $3.608n$ | $6.250n$ |
| Longeron **C** | $1.782n$ | 0 | $7.217n$ | 0 | $7.217n$ | 0 |
| Diagonal **AB** | $0.0315n$ | 8.839 | 0 | 17.68 | 0 | 17.68 |
| Diagonals **BC** and **CA** | $0.0158n + 7.655$ | 4.419 | 15.31 | 8.839 | 15.31 | 8.839 |
| Batten **AB** | $0.0446n$ | 0 | 0 | 0 | 0 | 0 |
| Battens **BC** and **CA** | $0.0223n$ | 0 | 0 | 0 | 0 | 0 |

**Table 6 Summary comparison of design alternatives for three bay numbers *n***

| Number of bays | $n$ | 30 | | | 60 | | | 90 | | | |
|---|---|---|---|---|---|---|---|---|---|---|---|
| Design in Fig. 2 | | Figure 2a | Figure 2b | Figure 2c | Figure 2a | Figure 2b | Figure 2c | Figure 2a | Figure 2b | Figure 2c | |
| Maximum slewing load, diagonal | $F_{d,s}$ | 8.839 | 17.68 | 17.68 | 8.839 | 17.68 | 17.68 | 9.073 | 17.68 | 17.68 | N |
| Parasitic diagonal loads | $F_{d,eT}$ | 59.31 | | | 59.31 | | | 59.31 | | | N |
| Tendon pretension required | $F_p$ | 68.65 | 18.18 | 18.18 | 68.65 | 18.18 | 18.18 | 68.88 | 18.18 | 18.18 | N |
| Maximum diagonal force | $F_{\max,d}$ | 136.8 | 35.86 | 35.86 | 136.8 | 35.86 | 35.86 | 137.3 | 35.86 | 35.86 | N |
| Dynamically optimal pretension | $F_{p,f}$ | 111.5 | 111.5 | 111.5 | 446.1 | 446.1 | 446.1 | 1004 | 1004 | 1004 | N |
| Batten Euler load | $F_{\mathrm{eu},p}$ | 709.5 | 709.5 | 709.5 | 2838 | 2838 | 2838 | 6385 | 6385 | 6385 | N |
| Long. strength degradation | $C_e$ | | 0.969 | 0.969 | | 0.984 | 0.984 | | 0.990 | 0.990 | N |
| Parasitic longeron loads | $F_{l,eT}$ | 83.87 | | | 83.87 | | | 83.87 | | | N |
| Longeron preload | $F_{l,p}$ | 97.09 | 25.71 | 25.71 | 97.09 | 25.71 | 25.71 | 97.41 | 25.71 | 25.71 | N |
| Longeron deployment penalty | $F_{l,\mathrm{depl}}$ | 181.0 | 25.71 | 25.71 | 181.0 | 25.71 | 25.71 | 181.3 | 25.71 | 25.71 | N |
| Base phased-array rms error | $\varepsilon_{\mathrm{rms}}$ | | 0.144 | 0.173 | | 0.072 | 0.087 | | 0.048 | 0.058 | mm |

## VI. Truss Beam Equivalent Stiffnesses

Stiffness is often of paramount importance for space applications, and it is of a special concern for laced trusses because it is profoundly affected by member cross section reduction. The more slender (some of the) members, the lower their stiffness, and the higher the compliance of the truss as a whole. Further, in diagonally laced beams, the members replaced with tendons (the diagonals) primarily and directly define global shear and torsional response. Accordingly, the assessment of effective shear and torsional stiffnesses must be performed with care.

Shear compliance also necessitates that considerations be based on the Timoshenko assumptions [19–21], which permit cross-sectional shear deformations. This premise is implied herein.

### A. Summary of Equivalent Stiffnesses

The equivalent beam stiffnesses for the designs concerned in this paper are listed in Table 7. The expressions, worked out independently for the present paper, agree with previously published results [12] when available and appropriate (for the rotationally symmetric determinate design save the shear results, and for the redundant design).

However, the rigorously formulated shear stiffnesses for the rotationally symmetric determinate design (Fig. 2b) turn out to differ from the results available in the literature. The difference is due to a conceptual error in a seminal study nearly three decades ago. This error is explained in Appendix A, in which a correct derivation for the shear stiffness is presented. The stiffness derivations for the determinate design with mirror symmetries (Fig. 2c) only differ from those of the rotationally symmetric design in minor details. Accordingly, they are not detailed herein.

Shown in Table 7 are all the Timoshenko beam equivalent stiffnesses: those for axial load, flexure, shear, and torsion. None of the results depend on the cross-sectional orientation $(x, y)$. A noteworthy detail is that the last design (Fig. 2c) is torsionally stiffer than its rotationally symmetric alternative (Fig. 2b). This is due to the more circuitous torsion-load path for the rotationally symmetric configuration: there, the diagonal forces that bear the torque need to be balanced at the joints by a tension-compression pattern that involves all three longerons. For the design with the disturbed symmetry, only the longeron across the flipped side (longeron **B** in Fig. 2c) bears loads, because the diagonal loads at the joints on the other longerons balance. By disturbing the rotational symmetry, shortcuts in the load path were created and the consequent elimination of loads in two of the longerons has improved performance.

### B. Example Designs

The equivalent beam cross-sectional stiffnesses for the example truss designs considered in the previous sections are listed in Table 8. As the symbolic relations in Table 7 also reveal, the axial and shear stiffness values $\hat{K}_F$ and $\hat{K}_S$ do not depend on the bay number $n$ (or on the truss depths), whereas the flexural stiffness $\hat{K}_M$ varies with the inverse second power of this parameter. The two determinate designs differ only in their torsional stiffnesses $\hat{K}_Q$. As previously revealed in Table 7, the torsional stiffness of the determinate design with the perturbed symmetry (Fig. 2c) is indeed higher than that of the fully

**Table 7 Beam stiffnesses for axial load $\hat{K}_F$, shear $\hat{K}_S$, flexure $\hat{K}_M$, and torsion $\hat{K}_Q$ (cf. *EA*, *GA*, *EI*, and *GJ*)**

| Cross-sectional stiffness | Redundant (Fig. 2a)[a,b] | Determinate 120-deg rotational symmetry (Fig. 2b)[b] | Determinate limited mirror symmetry (Fig. 2c)[b] |
|---|---|---|---|
| $\hat{K}_F$ | $3K_lB$ | $3K_l$ | $3K_l$ |
| $\hat{K}_S$ | $3\lambda_b^2\lambda_lK_d$ | $(3/2)\lambda_b^2\lambda_lK_d$ | $(3/2)\lambda_b^2\lambda_lK_d$ |
| $\hat{K}_M$ | $l_b^2K_l(3+B)/8$ | $l_b^2K_l/2$ | $l_b^2K_l/2$ |
| $\hat{K}_Q$ | $2C$ | $C/[1+\lambda_l^3K_d/K_l]$ | $C/[1+\lambda_l^3K_d/(3K_l)]$ |

[a] $B = 1/[1-2\lambda_l^3/(K_lC_k)]$.
[b] $C = \lambda_b^3l_ll_bK_d/4$.

**Table 8 Stiffness performance for design alternatives for three bay numbers *n***

| Number of bays | | $n$ | 30 | | | 60 | | | 90 | | | |
|---|---|---|---|---|---|---|---|---|---|---|---|---|
| Design in Fig. 2 | | | Figure 2a | Figure 2b | Figure 2c | Figure 2a | Figure 2b | Figure 2c | Figure 2a | Figure 2b | Figure 2c | |
| *Equivalent beam cross-sectional stiffnesses* | | | | | | | | | | | | |
| Axial load (cf. *EA*) | $\hat{K}_F$ | | 18,490 | 17,610 | 17,610 | 18,490 | 17,610 | 17,610 | 18,490 | 17,610 | 17,610 | kN |
| Shear (cf. *GA*) | $\hat{K}_S$ | | 471.8 | 235.9 | 235.9 | 471.8 | 235.9 | 235.9 | 471.8 | 235.9 | 235.9 | kN |
| Flexure (cf. *EI*) | $\hat{K}_M$ | | 32,020 | 32,610 | 32,610 | 8254 | 8152 | 8152 | 3668 | 3623 | 3623 | kN-m$^2$ |
| Torsion (cf. *GJ*) | $\hat{K}_Q$ | | 873.7 | 425.5 | 433.0 | 218.4 | 106.4 | 108.2 | 97.08 | 47.27 | 48.11 | kN-m$^2$ |
| *Deformation of a half-truss beam under* $\beta = 10^{-3}$ rad/s$^2$ *slew* | | | | | | | | | | | | |
| Tip deflection | $e_{\mathrm{tip}}$ | | 14.34 | 15.83 | 15.83 | 53.39 | 55.36 | 55.36 | 118.5 | 121.2 | 121.2 | mm |

symmetric design (Fig. 2b). Although this difference is minor (less than 2%), the very existence of a benefit of symmetry perturbation is noteworthy.

Also listed in the table are the cantilever tip deflections for half the truss beams (from the midspan out) under the condition considered in Table 5. Namely, the trusses are subject to a steady-state rotational (slew) acceleration of $\beta = 10^{-3}$ rad/s$^2$ from a torque applied at midspan. According to the Timoshenko condition, the tip deflection $e_{\text{tip}}$ is a combination of a flexural $e_{\text{tip},M}$ and a shear $e_{\text{tip},S}$ component:

$$e_{\text{tip}} = e_{\text{tip},M} + e_{\text{tip},S} \tag{36}$$

$$e_{\text{tip},M} = 11\beta\rho_L L^5/(3840\hat{K}_M) \tag{37}$$

$$e_{\text{tip},S} = \beta\rho_L L^3/(24\hat{K}_S) \tag{38}$$

The deflections vary from 14 mm through 12.1 cm, depending on the bay number (truss depth) and the design. The numbers are indicative of both the different stiffness performances of the deterministic and indeterminate designs (somewhat better performance for the latter) and of the dramatic impact of the truss depth (higher bay number, lower depth, and lower stiffness). The deflections for the two deterministic designs do not differ.

## VII. Conclusions

Fundamental considerations and relations for the design of a generic class of diagonally laced lattice beams were reviewed. Three prismatic triangular beams (an indeterminate design with identical doubly laced bays and two determinate designs with two-bay repeating units and different lacing patterns) were examined. The results were quantified in the context of 100-m-long square-bayed space truss examples with the number of bays varied.

In the indeterminate design, the pretension required for tendon tautness under mission conditions was shown to be heavily penalized by parasitic loads due to environmental and imperfection effects. Higher pretension consequently results in higher member loads and the need for a more forceful deployment mechanism. On the other hand, the determinate alternatives can accommodate low prestress but, in turn, undergo higher distortions as a result of kinematic effects. These deformations were shown to vary with the lacing pattern.

The distortions in either determinate structure also render the compression eccentric in the longerons if the latter are connected to one another in a flexurally stiff manner across the truss joints. This effect may be nonnegligible in realistic conditions.

Some issues related to the assessment of equivalent continuum beam stiffnesses were also discussed. Along with a review of formulas applicable for the trusses herein considered, a shear stiffness formula commonly used was revealed as erroneous, and the error was corrected.

In addition to the direct benefits in the context of the considered triangular truss designs of the considerations and relations presented, the present work also offers a blueprint for the design of any tendon-stiffened truss column. The practical value of this blueprint as a "design guide" will grow in the future as larger deployable space structures are considered, because classic off-the-shelf deployable truss beam systems (or concepts) cannot be applied to ever-increasing dimensions. Consequently, many large future systems will be designed individually from scratch, a process greatly aided by a systematic review of various design issues such as the one herein offered.

## Appendix A: Derivation of Equivalent Beam Shear Stiffness

For the truss architectures considered in the present paper, all beam equivalent cross-sectional stiffnesses were independently derived. The results generally confirmed the formulas known from earlier publications when applicable, with the exception of the cross-sectional shear stiffnesses of the determinate trusses, which are constructed of two-bay repetitive units.

This discrepancy stems from an error in a derivation carried out in a study decades ago [12]. Because this error is conceptual, not algebraic or symbolic, its illumination and correction calls for a discussion of the philosophical fundamentals of truss and beam modeling. The derivation detailed here must therefore begin with a discussion of conceptual fundamentals and their history.

### I. Continuum Beam Model

Linear lattices (truss beams) are often modeled as continuous beams to generate simple and transparent solutions, often in closed form and with back-of-the-envelope elegance. If the right beam parameters are used, the results well-represent quasi-static deformation or transient response. (Continuum models, however, can produce grossly nonconservative errors in stability analysis [22].)

For simple prismatic truss beams, one can derive the equivalent beam parameters with modest effort, or one can rely on published formulas. Although these formulas, scattered in a rather rich body of literature [23], are most often obtained via direct symbolic calculations of member loads and deformations, other, less usual, approaches are also available (e.g., the direct numerical testing of lattice sections [24] or the experimental refinement of preliminary predictions [25]).

Two studies discussing the derivation and values of equivalent beam parameters are of special significance for our present focus. The first, by Noor et al. [12], formally embeds the struts in a virtual continuum by calculating strut deformations (subsequently, loads) from the kinematic equations of a continuum. The other, included in relevant chapters of Renton's book [26], ultimately places truss beam analysis on the rigorous foundation of difference equations. Here, we pay particular attention to these seminal works, not only because of their continuing influence on engineering (an influence due to their comprehensive scope, intellectual elegance, and theoretical rigor), but also because they both disseminate an error in the calculation of shear stiffness for the kind of trusses considered in this paper. Namely, the equivalent cross-sectional shear compliance values for two-bay repetitive lattice beam architectures such as those in Figs. 2b and 2c in the body of this paper are derived with an error in the Noor et al. paper [12], and the same error is inherited by Renton's work [26]. This error does not affect the other lattice beam results presented in the concerned publications (the results related to one-bay repetitive architectures and to the axial, torsional, and purely flexural parameters of two-bay repetitive truss beams).

### II. Cross Sections: Shear and Flexure

Of the fundamental abstractions from which beam theory is constructed (member loads, deformations, and the very notion of the rigid cross section itself), one can consider shear to be the most conceptual. This is so because a beam of finite length cannot be subject to shear alone. It can be compressed, flexed, or twisted exclusively and singularly, but it can be sheared only if flexure (precisely, nonconstant flexure) is also present. Shear, proportional to the first derivative with respect to the beam "arc" length of the bending moment, is auxiliary to flexure.

It also happens that the inclusion of shear effects in beam theory pushes the latter to the limit, where its fundamental assumption of rigid cross sections (which would strictly imply constant shear deformation and stress: constant $\gamma = \tau/G$ over each cross section) becomes untenable. The shear coefficient introduced to negotiate this contradiction is but a fudge factor that has been the subject of ongoing dialogue until recently [20,27–30], despite some 80 years since shear was formally integrated into beam theory [19].

However, regardless of the complications consequent to this tenet, beam shear strictly entails the kinematics shown in Fig. A1a: the cross sections uniformly "slide" like a stack of cards, resulting in a (small) shear angle $\gamma = u/l$. The cross sections do not pivot; points such as **P** are not displaced along the beam axis. This kinematics, which can occur in its pure form for an infinitesimal beam length

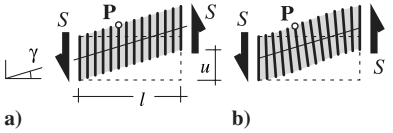


**Fig. A1 Shear vs shear combined with flexure.**

only, necessarily combines with (adds upon) the flexural kinematics (cross-sectional rotations and consequent cumulative lateral displacements) in any realistic context. This principle of superposition (the linear combination of the *abstractly pure* shear kinematics with the flexural deformations) underlies shear–flexural beam modeling.

### A. *Shear Stiffness According to Noor*

The principle of *abstractly pure* shear in shear response considerations (to be superimposed on the flexural response) just stated is violated, for example, if the supposed shear response is evaluated not in the abstract, pure, context but with a model that already combines it with flexure effects. This happens if axial displacements such as that of point **P** in Fig. A1b are permitted. This very mistake is made by Noor et al. [12]. In his analysis of the lattice cell (the "repeating element"), from the Taylor series that describes the kinematics he carefully employs components to *not constrain* motion to the boundary between the two bays. This lets the joints in the middle of the repeating element move freely even along the beam axis. In support of this approach, he shows the example of axial load [12] (Fig. 3, page 1223), in which lateral displacement of the interbay joints indeed must be allowed for the expected (zigzag) displacement pattern to develop. However, he consequently states that "local deformation should be allowed to occur freely" for the analysis of *all* complex (such as two-bay) cells. As a result of this inappropriate generalization, he then permits the internal nodes of a two-bay cell to move axially even when the cell is subjected to shear alone. Shown via a planar example in Fig. A2, this scenario combines shear with flexure as its continuum analogy (Fig. A1b). Shear stiffness is consequently underestimated by the expression then derived for the design referred to here as the rotationally symmetric bracing options (Fig. 2b) as

$$\hat{K}_S = \frac{3\lambda_b^2\lambda_l K_d}{2 + \lambda_l^3 K_d/(2K_l)} \tag{A1}$$

cited here from row 3 and column 4 of Table 1 by Noor et al. [12] (page 1222), expressed with the variables used in the present paper. The second term in the denominator, containing the longeron stiffness $K_l$, is superfluous.

### B. *Correct Shear Stiffness*

As stated in the body of this paper, the correct shear stiffness for design Fig. 2b (and, incidentally, Fig. 2c) is

$$\hat{K}_S = (3/2)\lambda_b^2\lambda_l K_d \tag{A2}$$

rather than Eq. (A1). This formula was first derived for the present paper from elementary kinematic and mechanical considerations in the correct context of *one single* truss bay. (The same approach was used for the derivation of the other formulas listed in Table 7.) This derivation explicitly relies on the mechanical arguments detailed in the preceding subsections: philosophical arguments that define the consequent arithmetic and, concurrently, constitute the very difference between the route followed by Noor et al. [12] and the trail blazed here. By virtue of this fundamental difference in approach, Eq. (A2) should naturally differ from the Noor result, regardless of which is correct.

To properly verify Eq. (A2), an additional derivation of the shear stiffness without philosophical–conceptual arguments such as those detailed in Appendix A (Secs. A.II and A.II.B) is necessary. To this end, we develop an exact closed-form solution for the tip deflection $e$ of a laterally loaded truss cantilever of architecture Fig. 2b and then compare the relation obtained with predictions via Eqs. (A1) and

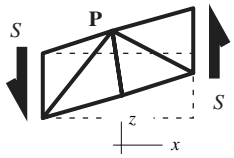


**Fig. A2 Shear of internally unconstrained cell.**

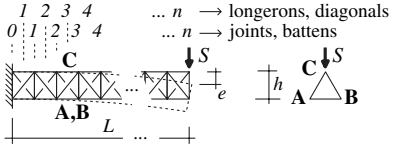


**Fig. A3 Tip-loaded cantilever lattice beam.**

(A2). As indicated in Fig. A3, the number of bays (longerons and diagonals) is $1, \ldots, n$, and the joints and battens are $0, \ldots, n$ from support to tip. The longerons are distinguished with letters **A**, **B**, and **C**. Let $n$ be even.

To calculate the tip deflection $e$, begin with the member loads (derived from equilibrium considerations)

$$\begin{aligned}
F_{l,A} &= -S\lambda_l[n + 1 - 2\,\mathrm{int}(i/2 + 1/2)]/(\sqrt{3}\lambda_b)\\
F_{l,B} &= -S\lambda_l[n - 2\,\mathrm{int}(i/2)]/(\sqrt{3}\lambda_b)\\
F_{l,C} &= +S\lambda_l[2n + 1 - 2i]/(\sqrt{3}\lambda_b)\\
F_{b,AB} &= F_{b,BC} = 0\\
F_{b,CA} &= 0 \qquad \text{for } i < n\\
F_{b,CA} &= -S/\sqrt{3} \qquad \text{for } i = n\\
F_{d,AB} &= 0\\
F_{d,BC} &= -S(-1)^i/(\sqrt{3}\lambda_b)\\
F_{d,CA} &= +S(-1)^i/(\sqrt{3}\lambda_b)
\end{aligned} \tag{A3}$$

where int( ) is the *integer part* function and $i$ is the bay number (cf. Fig. A3). The tip displacement can then be obtained by substituting the member loads $F_i$ from Eq. (A3) into

$$e = S^{-1}\sum(F_i^2 l_i/K_i) \tag{A4}$$

which is a general expression for a displacement under a single load, easily obtained from energy principles.

By developing the squares, converting the resulting arithmetic and power progressions to closed-form expressions, and then rearranging, one obtains

$$\begin{aligned}
e &= \sum\{[F_{l,A}^2 + F_{l,B}^2 + F_{l,C}^2]l_l/(SK_l)\} + F_{b,CA,i=n}^2 l_b/(SK_b)\\
&\quad + \sum\{[F_{d,BC}^2 + F_{d,CA}^2]l_d/(SK_d)\}\\
&= S/3[2n^3\lambda_l^2 l_l/(\lambda_b^2 K_l) + l_b/K_b + 2l_d n/(\lambda_b^2 K_d)]\\
&= S/3[2L^3/(l_b^2 K_l) + L\lambda_b/(n\lambda_l K_b) + 2L/(\lambda_l\lambda_b^2 K_d)]
\end{aligned} \tag{A5}$$

The first term of the final expression, $2SL^3/(3l_b^2 K_l)$, is the longeron contribution: it precisely corresponds to Euler–Bernoulli flexure [$e = SL^3/(3EI)$] with equivalent flexural stiffness $K_l l_b^2/2$, as also stated by Noor et al. [12] (row 2, column 4 of Table 1, page 1222). The second term, $L\lambda_b/(n\lambda_l K_b)$, reflects the local effects at the cantilever tip: a Saint-Venant term, which diminishes if $n$ increases for a given $L$. The last term, $2SL/(3\lambda_l\lambda_b^2 K_d)$, is the diagonal (shear) contribution: it exactly corresponds to the *correct* shear stiffness of the equivalent beam [Eq. (A2)]. Thus, the result derived for the present paper, Eq. (A2), is verified.

For yet another independent control, a simple finite element model of a truss such as in Fig. 2b was also built and its cantilever deflection under lateral load was evaluated. The result agreed with Eq. (A5) with numerical accuracy. The details of this exercise, of minor importance after the theoretical and formal considerations have already been detailed, are not discussed herein.

We conclude that the shear coefficient by Eq. (A1) overestimates compliance with the factor

$$1 + \lambda_l^3 K_d/(4K_l) \tag{A6}$$

This is a nearly 9% error for square bays ($\lambda_l = 1/\sqrt{2}$) and uniform members ($K_d = K_l$). However, this amplification is attenuated if the diagonals are reduced. In formal terms, $\lambda_l^3 K_d/(4K_l) \to 0$ if $K_d \to 0$.

### C. Note on Shear Stiffness According to Renton

In his treatise, Renton [26] offers valuable insight into the lattice-continuum analogy in Chapters 8, 15, and A-5. He derives equivalent beam stiffnesses with finite difference calculus, an eloquent and rigorous tool to solve repetitive lattices. However, he makes the same mistake as Noor et al. [12] in the shear analysis of lattices of multibay modules, loading the latter with shear at the module ends, with the internal nodes unconstrained. This error affects the shear stiffnesses quoted for the German SPAS system on page A5.7, paragraph S5 of [26], and more results from an earlier publication [31], from where the SPAS parameters are quoted.

### D. Concluding Comments

Of truss beam equivalent continuum properties, the shear stiffnesses of lattices with multibay cells are the only ones in which widely quoted results tend to err. The other stiffness coefficients in the literature are generally reliable. Consequently, when assessing shear stiffness for the architectures in Figs. 2b and 2c, one should use Eq. (A2), rather than alternative expressions. For the other beam parameters (all coefficients for design Fig. 2a and the flexural, torsional, and axial coefficients for Figs. 2b and 2c), the results available in the literature are appropriate.

As a general rule, one should remember that a continuum analogy should be built around the lattice unit most closely analogous to the defining abstraction of the continuum model. For a beam, this abstraction is the cross section, and the most closely analogous lattice unit in common trusses is the bay, not the repeating cell. If the bays are not uniform, the appropriate model may be a beam of nonuniform stiffness.

A rigorous derivation according to the principles just stated, nevertheless, may still resemble the Noor et al. [12] approach in several ways. As repeating nonuniformities level out over the beam length, a model may be constructed to reflect the resultant effective value, rather than local variations. Also, there is nothing inherently wrong in a calculation spanning several bays, as long as consistency with the addressed truss and beam behavior is rigorously maintained. And, of course, care should be taken to not constrain possible secondary kinematics coupled with the considered beam effect, as Noor et al. [12] point out. However, motion inconsistent with the studied beam response should not be allowed.

## Acknowledgments

This work was partly supported by L'Garde, Inc., under a project managed by Yuki Michii, Art Palisoc, Billy Derbes, and Gordon Veal. The author thanks Tom Murphey for his help in identifying and sharing some of the references cited. The help of Yuki Michii for a review of the composition of arguments and for eliminating typos is also gratefully acknowledged.

## References

[1] Miura, K., and Tanizawa, K., "Tension Truss Antenna—Concept, Reality, and Future," *IUTAM–IASS Symposium on Deployable Structures: Theory and Applications*, edited by S. Pellegrino and S. D. Guest, Solid Mechanics and Its Applications, Vol. 80, Kluwer Academic, Dordrecht, The Netherlands, 2000, pp. 291–300.

[2] Thomson, M. W., "The AstroMesh Deployable Reflector," *Proceedings of the 5th International Mobile Satellite Conference (IMSC '97)*, Jet Propulsion Lab., California Inst. of Technology, Pasadena, CA, 16–18 June 1997, pp. 393–398; also Jet Propulsion Lab., Paper 97-11, 1997.

[3] Tibert, A. G., and Pellegrino, S., "Deployable Tensegrity Reflectors for Small Satellites," *Journal of Spacecraft and Rockets*, Vol. 39, No. 5, Sept.–Oct. 2002, pp. 701–709.

[4] Eiden, M., Brunner, O., and Stavrinidis, C., "Deployment Analysis of the Olympus Astromast and Comparison with Test Measurements," *Journal of Spacecraft and Rockets*, Vol. 24, No. 1, Jan.–Feb. 1987, pp. 63–68.

[5] Murphy, D. M., Murphey, T. W., and Gierow, P. A., "Scalable Solar Sail Subsystem Design Considerations," 43rd AIAA Structures, Structural Dynamics, and Materials Conference and Exhibit, Denver, CO, AIAA Paper 2002-1703, 2002.

[6] Okazaki, K., Sato, S., Obata, A., Natori, M., and Miura, K., "Design Consideration of Mechanical and Deployment Properties of a Coilable Lattice Mast," *Proceedings of the 15th International Symposium on Space Technology and Science*, AGNE Publishing, Tokyo, May 1986, pp. 497–502.

[7] Levine, M. B., "Microdynamic Behavior of a Joint Dominated Structure On-Orbit," 39th AIAA Structures, Structural Dynamics, and Materials Conference and Exhibit, Long Beach, CA, AIAA Paper 1999-1267, 1999.

[8] Warren, P. A., Hinkle, J. D., and Harvey, T. J., "Decent Developments in High Efficiency, Elastically Deployed Boom Structures," 44th AIAA Structures, Structural Dynamics, and Materials Conference and Exhibit, Norfolk, VA, AIAA 2003-1823, 2003.

[9] Onoda, J., "Two-Dimensional Deployable Truss Structures for Space Applications," *Journal of Spacecraft and Rockets*, Vol. 25, No. 2, Mar.–Apr. 1988, pp. 109–116.

[10] Takamatsu, K. A., and Onoda, J., "New Deployable Truss Concepts for Large Antenna Structures or Solar Concentrators," *Journal of Spacecraft and Rockets*, Vol. 28, No. 3, May–June 1991, pp. 330–338.

[11] Onoda, J., Fu, D.-Y., and Minesugi, K., "Two-Dimensional Deployable Hexapod Truss," *Journal of Spacecraft and Rockets*, Vol. 33, No. 3, May–June 1996, pp. 416–421.

[12] Noor, A. K., Anderson, M. S., and Greene, W. H., "Continuum Models for Beam- and Platelike Lattice Structures," *AIAA Journal*, Vol. 16, No. 12, Dec. 1978, pp. 1219–1228.

[13] Murphey, T., and Hinkle, J., "Some Performance Trends in Hierarchical Truss Structures," 44th AIAA Structures, Structural Dynamics, and Materials Conference and Exhibit, Norfolk, VA, AIAA Paper 2003-1903, 2003.

[14] Greene, W. H., "A Design Procedure for a Tension-Wire Stiffened Truss-Column," NASA Langley Research Center, Rept. CR-3273, Hampton, VA, Apr. 1980.

[15] Hetényi, M., *Beams on Elastic Foundation. Theory with Applications in the Fields of Civil and Mechanical Engineering*, Univ. of Michigan Press, Ann Arbor, MI, 1946.

[16] Shaker, F. J., "Effect of Axial Load on Mode Shapes and Frequencies of Beams," NASA Lewis Research Center TN D-8109, Cleveland, OH, Dec. 1975.

[17] Greschik, G., Mikulas, M. M., Helms, R. G., and Freeland, R. E., "Strip Antenna Figure Errors Due To Support Truss Member Length Imperfections," 45th AIAA Structures, Structural Dynamics, and Materials Conference and Exhibit, Palm Springs, CA, AIAA Paper 2004-1601, 2004.

[18] Peterson, J. P., Seide, P., and Weingarten, V. I., "Buckling of Thin-Walled Circular Cylinders," *NASA Space Vehicle Design Criteria: Structures* NASA Langley Research Center Rept. NASA SP-8007, Hampton, VA, Aug. 1968.

[19] Timoshenko, S. P., "On the Correction for Shear of the Differential Equation for Transverse Vibration of Prismatic Bars," *Philosophical Magazine*, Vol. 41, 1921, pp. 744–746; reprint, *The Collected Papers of Stephen P. Timoshenko*, McGraw–Hill, London, 1953.

[20] Wang, C. M., "Timoshenko Beam-Bending Solutions in Terms of Euler-Bernoulli Solutions," *Journal of Engineering Mechanics*, Vol. 121, No. 6, June 1995, pp. 763–765. doi:10.1061/(ASCE)0733-9399(1995)121:6(763)

[21] Hlavaček, I., "Buckling of a Timoshenko Beam on Elastic Foundation with Uncertain Input Data," *IMA Journal of Applied Mathematics*, Vol. 68, No. 2, 2003, pp. 185–204. doi:10.1093/imamat/68.2.185

[22] Razdolsky, A. G., "Euler Critical Force Calculation for Laced Columns," *Journal of Engineering Mechanics*, Vol. 131, No. 10, Oct. 2005, pp. 997–1003. doi:10.1061/(ASCE)0733-9399(2005)131:10(997)

[23] Noor, A. K., and Mikulas, M. M., "Continuum Modeling of Large Lattice Structures: Status and Projections," *Large Space Structures: Dynamics and Control*, edited by Atluri, S. N. and Amos, A. K., Springer Series in Computational Mechanics, Springer–Verlag, New York, Apr. 1988, pp. 1–34.

[24] Sun, C. T., and Kim, B. J., "On the Derivation of Equivalent Models for Beam- and Plate-Like Structures," *AIAA Dynamic Specialists Conference*, AIAA, New York, 1981, pp. 523–532; also AIAA Paper 1981-0624.

[25] Sun, C. T., and Juang, J. N., "Modeling Global Structural Damping in Trusses Using Simple Continuum Models," *AIAA Journal*, Vol. 24, No. 1, Jan. 1986, pp. 144–150.

[26] Renton, J. D., *Elastic Beams and Frames*, 2nd ed., Engineering Science, Horwood Publishing, Chichester, England, U.K., 2002.

[27] Hutchinson, J. R., "Shear Coefficients for Timoshenko Beam Theory," *Journal of Applied Mechanics*, Vol. 68, No. 1, Jan. 2001, pp. 87–92. doi:10.1115/1.1349417

[28] Stephen, N. G., "Discussion: 'Shear Coefficients for Timoshenko Beam Theory'," *Journal of Applied Mechanics*, Vol. 68, No. 6, Nov. 2001, pp. 959–960. doi:10.1115/1.1412454

[29] Hutchinson, J. R., "Closure to 'Shear Coefficients for Timoshenko Beam Theory'," *Journal of Applied Mechanics*, Vol. 68, No. 6, Nov. 2001, pp. 960–961. doi:10.1115/1.1412455

[30] Rubin, M. B., "On the Quest for the Best Timoshenko Shear Coefficient," *Journal of Applied Mechanics*, Vol. 70, Jan. 2003, pp. 154–157. doi:10.1115/1.1526122

[31] Renton, J. D., "The Beam-Like Behavior of Space Trusses," *AIAA Journal*, Vol. 22, Feb. 1984, pp. 273–280.

J. Wei
*Associate Editor*